J Therm Anal Calorim (2013) 111:857–867
DOI 10.1007/s10973-012-2195-8

Sensor placement in temperature-based control strategies to improve baseline stability in Tian–Calvet microcalorimeters

Luis E. Vilchız-Bravo · Arturo Pacheco-Vega · Brent E. Handy

Received: 19 October 2011 / Accepted: 3 January 2012 / Published online: 22 January 2012

Abstract We address the issue of hardware placement in the development of robust temperature control strategies that can be used to maintain a stable baseline during microcalorimetric experiments. The two different control loops, each defined by the location of sensor within the calorimeter that is used to achieve control, were first developed and then tested in a fully instrumented experimental system. Both control strategies were structured on proportional-integral-derivative controllers, after which calorimetric experiments were carried out to test the efficiency and robustness of the corresponding methodology. Results indicate that sensor placement plays a fundamental role in the controlled baseline stability and that is better to place the sensing device closer to the heater than to the central core. As part of this study, comparisons were also done against a previously reported control scheme based on heat-flow measurements. Results indicate that controlling only one variable, either temperature or heat flow is sufficient to compensate for heater-induced noise, but not for external fluctuations for which a combined strategy may be necessary.

L. E. Vilchız-Bravo
Facultad de Ingeniería Química, Universidad Autónoma de Yucatán, 97203 Mérida, YUC, México

A. Pacheco-Vega (✉)
Department of Mechanical Engineering, California State University Los Angeles, Los Angeles, CA 90032, USA
e-mail: apacheco@calstatela.edu

B. E. Handy
CIEP-Facultad de Ciencias Químicas, Universidad Autónoma de San Luis Potosí, 78210 San Luis Potosí, SLP, México

Keywords Tian–Calvet microcalorimeter · Temperature control · Sensor placement · Baseline signal

List of symbols

e	Error signal
k_D, k_I, k_P	PID controller gains
$\mathcal{K}$	Calibration constant
L	Characteristic length
P	Electric power (W)
Q	Heat-flow rate (W)
T	Temperature (K)
T1	Temperature at T1 (K)
T2	Temperature at T2 (K)
t	Time
u_T	Input voltage signal (V)

Greek symbols

α	Thermal diffusivity (m^2/s)
δt	Time interval (s)
τ	Thermal lag

Subscripts and superscripts

p	Prediction
set	Setpoint
SHT	Heat-flow sensor
SP	Sample heat-flow sensing cup

Abbreviations

CDC	Continuously modulated direct-current
CTC	Conventional temperature control
DAQ	Data acquisition
DC	Direct current
HFC	Heat-flow control
PC	Personal computer
PID	Proportional-integral-derivative
PMS	Power modulation system

SHT	Heat-flow sensor
SP	Sample sensing cup
T1	Thermocouple in heat-sink unit
T2	Thermocouple close to SHT
TC	Tian–Calvet
SISO	Single-input single-output
SSR	Solid-state relay

Introduction

In the last three decades, heat-conduction calorimeters, also known as Tian–Calvet (TC), have experienced an increased interest to estimate enthalpy changes occurring in physicochemical processes. This enthusiasm has been motivated especially by technological advancements in the design and manufacturing of novel temperature-sensing devices and electronic components, which have produced better calorimetric instruments. Despite the fact that other types of calorimeters, like the isothermal and adiabatic instruments, are also frequently used in a variety of fields, including physics and chemistry, biology, biochemistry, pharmacology, and materials science, the TC design has been particularly convenient to examine relatively slow thermal processes associated with gas adsorption [1–4] necessary to characterize the properties of catalyst materials [5–9].

In a typical gas adsorption experiment above or below ambient temperature, a TC calorimeter uses a pair of heat-flux transducers—located between the sample holders and an ideally isothermal heat sink—to measure the unknown heat flow from a sample volume. The integrated heat flow over time provides the energy emitted during the thermal process. Differential measurements of the emitted heat between sample- and reference-cells are common to avoid baseline shifts and signal drift due to external thermal noise and internal power cycling [1, 3, 10]. It has to be noted, however, that the sample heat emissions being studied (and hence temperature changes) are often exceedingly small, causing the results of calorimetric measurements to be easily impaired by systematic errors related to calibration, baseline stability, and response time of the instrument [11, 12].

Different alternatives have been proposed in the literature to increase the detection limits of TC calorimeters. These range from studies of the design parameters [10, 13, 14], numerical simulations of the three heat transfer mechanisms occurring during gas dosing experiments [15], novel designs that use more sensitive thermistor elements [16], designs that either take advantage of a large thermal mass for implementing an inertial temperature control strategy [17] or use Peltier dynamic compensators with feed-back temperature control [18], among several investigations. Recently, Vilchiz et al. [19] reported upon the development of control strategies based on heat-flow and temperature measurements directed to increase the detection limits. Their results showed that a heat-flow control strategy provided a better baseline stability (with one order of magnitude noise reduction) than a typical temperature control scheme, though it was not as efficient in maintaining an isothermal core.

Here we take a step further in a research effort directed to increase the sensitivity of Tian–Calvet microcalorimeters, i.e., an experimental analysis on the role of sensor placement in the performance of temperature control methodologies used to maintain a stable baseline during microcalorimetric experiments. Two control strategies, based on the well-known proportional-integral-derivative (PID) scheme, are formulated upon the location of the sensor within the calorimeter. Experimental tests of the system dynamics and signal perturbation levels are then conducted in a fully instrumented microcalorimeter setup to assess the efficiency and robustness of each control strategy, as they relate to the position of the sensor, in attaining a stable baseline. Finally, comparisons of these strategies against a previously reported control scheme based on heat-flow measurements [19] and their performance under varying conditions external to the system were also carried out.

Experimental system

The Tian–Calvet calorimeter, a schematic of which is depicted in Fig. 1, is the same equipment used by Vilchiz et al. [19] to analyze the performance of the heat-flow and temperature control strategies that were previously developed with the goal of improving its baseline stability. The instrument was designed and built to operate at temperatures above 600 K which are necessary for high-temperature gas/solid adsorption tests.

In reference to Fig. 1, the calorimeter consists of an inner core manufactured of pure nickel that serves as a heat sink for heat emissions from specific sample materials. The inner-core block is surrounded by an outer shell built from stainless steel 304, and further by ceramic, fiber-glass, and brick-based insulation materials, required to minimize energy exchanges with the environment. Two thermopile units, of 3 mm wall thickness, 16 mm diameter $\times$ 20 mm-height cylindrical cup sensors (International Thermal Instruments Co., Del Mar, CA, USA), designated as sample- and reference-cells and located symmetrically in the inner core, are used to measure the heat-flow signals emitted during a gas adsorption experiment. A flat-plate electric heater that is anchored directly underneath the outer shell box supplies sufficient energy to the inner core to compensate for any heat losses to the environment. Feedback information to the temperature-based controllers

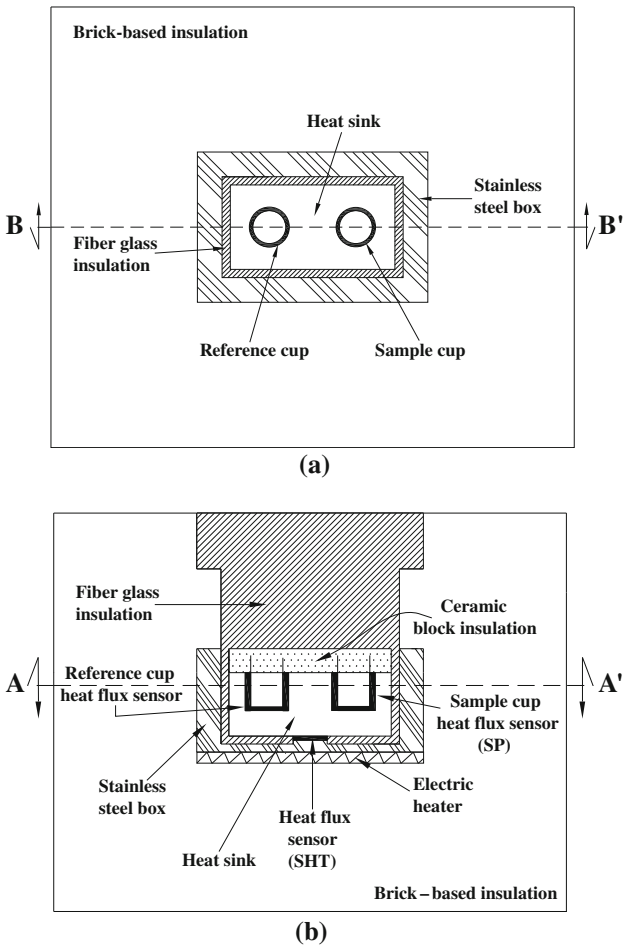

Fig. 1 Schematic of a Tian–Calvet calorimeter. **a** Section A–A′. **b** Section B–B′

under analysis was provided by either of two K-type thermocouples: The first (denoted as T1) is located at the centroid of the nickel heat sink, whereas the second (denoted as T2) is situated at midpoint between the heat-flux sensor (denoted SHT) and the electric heater. The heat-flux sensor SHT (Model HT-50, ITI Co., Del Mar, CA) was employed in a heat-flow-based controller scheme previously reported [19]. The chief goal of these control schemes was minimize the baseline heat-flow fluctuations sensed at the sample cups, detected at SP, subject to minimal drift in a set temperature value at T1. Good mechanical contact among all the components; i.e., the inner core, SHT, T2, the stainless steel box, and the heater, was ensured to minimize the contact thermal resistance. It should be noted that in the subsequent analyses, output signals from the sample-cup thermopile are referred as 'SP' while the feedback signals from the thermocouples are either denoted as 'T1' or 'T2'.

Figure 2 depicts the instrumentation for the experimental setup. It shows the flow of information from the sensors to the signal actuators and how the different subsystems; i.e., calorimeter, signal amplifiers, personal computer (PC) and data acquisition card (DAQ), and power-supply actuators are interconnected. This information comprises the heat emitted in the sample cell, the heat-sink temperature at the locations T1 and T2, and the energy supplied to the core unit by the electric heater, as acquired by the corresponding sensing elements, and time at which these were taken. Since the readings obtained from the thermocouple and thermopile sensors are at sub-microvolt levels, the analog values were amplified by two nanovoltmeters (Keithley 2182A) before being sent to the PC through a GPIB card. Inside the PC, LabVIEW software (National Instruments Co., Austin, TX USA) interfaced the test bed with the corresponding PID controller—which was coded using the subroutines built within the software—to first collect the measurements and then return the output signal to the system, after the controller had calculated the control action. A 16-channel data acquisition (DAQ) card received the digital output from the controller and provided the corresponding analog input to the electric heater by means of a power modulation system (PMS), using here a

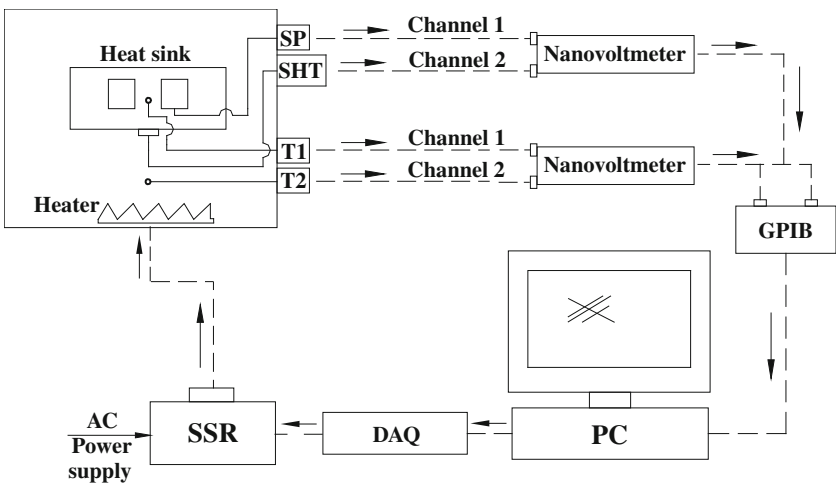

Fig. 2 Schematic of system instrumentation

solid-state relay (SSR) operating in a time-proportional ON-OFF mode. The unit was turned "ON" when the controller output exceeded 1.8 volts, resulting in an applied "ON" electric power of 134 W. It is important to note that the use of the Keithley nanovoltmeter in conjunction with the K-type thermocouple allows the experiments to achieve an ultimate resolution of ±0.001 K with an accuracy close to ±0.1 K. Power resolution for the heat-flow sensors, which are also coupled to the Keithley instrument, is confirmed via repetitive measurements to within ±0.5 mW for SP and ±2 mW for SHT. Additional details about the components, instrumentation and characteristics of the test bed are in Vilchiz-Bravo [20].

Temperature control schemes

In following our previous work [19], proportional-integral-derivative (PID) controllers are used as the basis for the thermal control of the experimental setup. Although other types of controllers are also feasible, e.g., those based on fuzzy logic [21] or artificial neural networks [22], the simplicity, good response, and low cost of PID-based control loops have motivated their popularity in industrial applications.

The two temperature control strategies implemented in this investigation, subsequently referred as CTC-T1 and CTC-T2, are displayed schematically in Fig. 3. From the figure it can be noticed that both closed-loop layouts are built upon information of the temperature obtained from the sensing devices; i.e., thermocouples—located at either the center of the calorimeter core (T1) or at a point between the core and the heater (T2)—and the power supplied by the heater unit to the system. This type of structure corresponds to a single-input single-output (SISO) system, with the temperature at T1 (or T2) as the system output and the power supply (i.e., voltage) being its input.

The goal of the PID controller, in either case, is to regulate the corresponding temperature toward specific values in response to changes in the external/internal conditions to/in the calorimeter. To achieve this goal, the controller provides an input signal to the electric heater which, in turn, supplies the necessary power to the calorimeter core unit. The controller output, u_{T}, which serves as the input signal (in volts) to the heater, is computed using the control law

$$u_{\mathrm{T}}(t+\delta t) = k_{\mathrm{P}} e_T(t) + k_{\mathrm{I}} \int_{t_0}^{t} e_T(z)dz + k_{\mathrm{D}} \frac{\partial e_T}{\partial t}, \qquad (1)$$

where e_T represents the difference (error) between the actual temperature reading, T, from the corresponding thermocouple (T1 or T2), and the desired set-point value T_{set}; i.e., $e_T(t) = T_{\mathrm{set}}(t) - T(t)$.

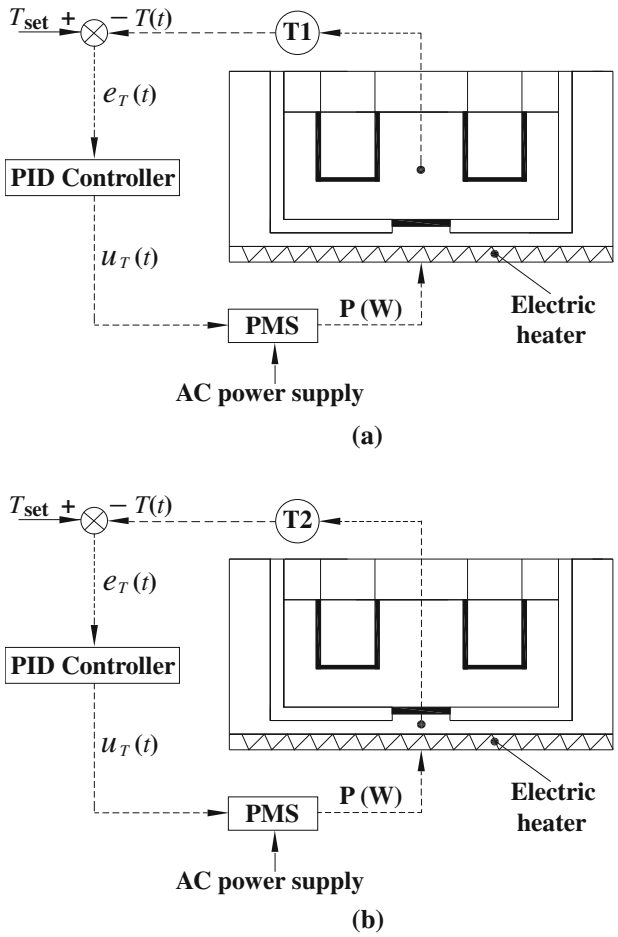

Fig. 3 Closed-loop temperature control schemes at T1 and T2. **a** CTC-T1 control. **b** CTC-T2 control

In the above equations, t represents time, k_{P}, k_{I}, and k_{D} are the proportional, integral, and derivative controller gains, respectively, and δt (=1.5 s) is the time that takes to process the data after they have been acquired. The double-tuning process of the controller gains via Cohen-Coon and Ziegler-Nichols techniques were described in detail earlier [19, 20].

To emphasize the importance of sensor placement in the control of the present calorimeter, a later section briefly describes the implementation of a previously reported heat-flow control scheme that provided a baseline stability better than that of the temperature control denoted here as CTC-T1.

Sensor placement in dynamics and control

The importance of hardware—sensor and/or actuator—location has been long recognized in several application

areas [23–26], particularly in those dealing with some form of system identification and/or control of distributed parameter systems, necessary to achieve a specific objective. Applications include the control of vibrating engineering structures [27, 28] and thermal-hydraulic networks [29], the development of structural monitoring and fault-detection systems [30, 31], computer vision [32], and thermal tracking [33]. In the tests reported next we show that sensor placement is fundamental for controlling the temperature to maintain a stable baseline during calorimetric experiments.

It should be noted that the results reported here are all based on the SSR actuator. Although the use of a CDC power-supply eliminates wide temperature and thermal power oscillations due to power cycling and time delays [19], these fluctuations are also virtually eliminated by locating the sensor closer to the actuator. Finally, to compare the advantages and disadvantages of the different control strategies, each was tested under similar conditions.

System response to a step-increase in power supply

The dynamic response of the calorimeter system to a step-like increase in the power supplied by the heater is depicted in Fig. 4. Shown are the temperature values sensed by the thermocouples located at T1 and T2, as well as the heat-flow values obtained by the appropriate heat-flow sensors SHT and SP, as they change in time. The initial values at T1 and T2 are 557.5 and 576.5 K, respectively. From the figure, some general features can be observed. The time-dependent curves for the temperature at locations T1 and T2 approximate a first-order system response, while those of the heat flow at both SP and SHT locations resemble the output of a second-order critically damped system. The T1 curve is smoother than the T2 trace and the SP heat-flow signal is attenuated with respect to SHT, both observations due to the damping effect of the thermal mass in the heat-sink element.

Immediately after the step change, the abrupt rise in the temperature at T2 at the onset coincides with an induction period in T1. Correspondingly, this behavior is reflected in the heat-flow measurements at SP and SHT, which show a spike at the early stages of the experimental test and a subsequent settlement to their corresponding steady-state levels of 2.15 W for SHT and 0.38 W for SP. After about 50 h, all the sensed signals have reached their steady-state values. As expected, the steady-state temperatures at T2 (=602.5 K) are higher than those at the central core T1 (=582.5 K) due to closer proximity of the T2 sensor to the energy source within the system; i.e., the electric heater. Since the settled values of the heat-flow signals are different from zero, and the temperatures reach different steady-state levels, it is clear that the system requires a sustained heat input to compensate for the energy losses to

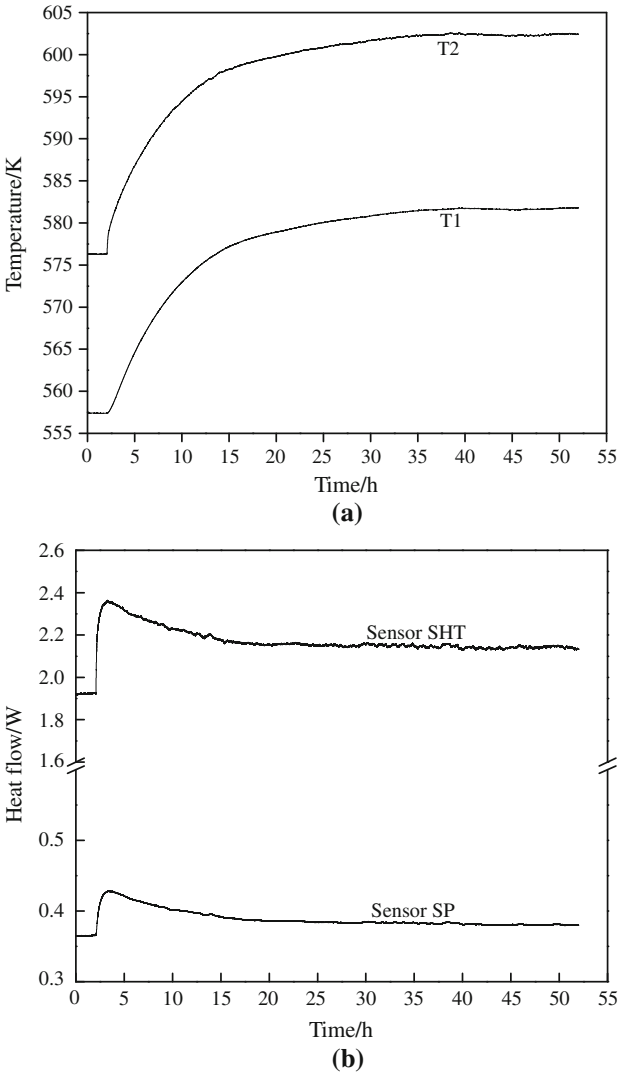

Fig. 4 System response due to a step-like increase in heater power. **a** Temperature measured at T1 and T2. **b** Heat flow measured at SHT and SP

the laboratory room. Actually, the heat-flow captured by the SHT sensor represents the net rate of energy transferred to the heat sink. The smaller magnitude of the heat-flow signal at SP is indicative that only a fraction of net rate of energy being transferred into the core is captured by this sensor. On average this fraction is 17.5% of the heat-flow signal at SHT.

Although not sufficiently clear due to the scale of Fig. 4, another important aspect that increases the complexity of the control problem of maintaining an isothermal core and a stable baseline at the calorimeter sensing cups is the thermal lag. Because of the locations of the different temperature and heat-flow sensors, and the fact that the energy transfer in the heat sink is purely via conduction, it can be noticed that the T1 and T2 signals (and SHT and SP traces) are displaced from each other by a time delay of

1.07 min. This experimental value is actually very close to the one estimated from scale analysis of the one-dimensional heat equation; i.e., $\tau = L^2/\alpha$, where τ is the time necessary for the energy to flow from the T1- to the T2-locations, and α is the thermal diffusivity for nickel, which comprises the heat sink, and L is the characteristic length of the heat-conduction problem (in this case is the distance between the temperature-sensing devices of 3.5 cm). The issue of thermal lag, and the need to minimize it, will become more apparent in the next sections.

System response under CTC-T1 and CTC-T2 control

Experimental results on sensor cup stability considered first temperature control, with the controlled temperature being either T1 (CTC-T1) or T2 (CTC-T2), whose locations are indicated in Fig. 3. To emphasize, thermocouple T1 was located at the geometric center of the calorimeter heat-sink core, whereas T2 was purposefully positioned as close as possible to the resistance heater plate to provide a relatively short time for sensing the heat being channeled to heat the core unit. Since we are interested in calorimetric experiments of catalyst materials, the set-points considered here for control via CTC-T1 and CTC-T2 are, respectively, 573.15 and 593.15 K. The set value for T1 corresponds to the mid-range values of the design temperature range that is used in isothermal calorimetry, whereas that of T2 arises from the corresponding reading obtained from the open-loop system response reported in the previous section.

The results from this run are shown in Fig. 5 for the case of CTC-T1, and in Fig. 6 for the case of CTC-T2. From the figures it can be seen that, after the usual settling period, both controllers maintain the temperature values well within ±0.1 K of the corresponding set-points; i.e., 573.15 K at T1 and 593.15 K for T2. Under CTC-T1, however, thermal cycling with a period of 3–4 min is considerable. This can be attributed to the ON-OFF cycling of the SSR power modulator, accentuated by the natural thermal lag in the calorimeter core. Since the T1 sensor is positioned relatively far from the actuator element (electric heater), the time delay (∼1 min) occurring between power supply at the bottom of the heat sink and temperature measurement at T1, significantly alters the control actions from the controller and the corresponding system response. Thermal power pulsing is similarly observed in the heat-flow signals collected at SP and SHT. In contrast, with the CTC-T2 strategy the amplitude is considerably lower, and the oscillation period shorter in temperature and heat-flow variations due to the heater power cycling, as recorded by all sensors, and approaches the uncertainty of the measurements. As noticed from Fig. 6, both T2 and SHT oscillate evenly with a period of 45 s, but this time, their amplitudes are five times smaller than those obtained under the application of CTC-T1. This is essentially the consequence of reducing the thermal lag by locating the temperature sensor closer to the actuator. Baseline heat-flow oscillations in SP, and the temperature variations at T1 under this control scheme are negligible, due to the effect of the heat sink thermal mass to more effectively time-average the smaller and more rapid oscillation pattern, compared to CTC-T1.

During the runs shown in Figs. 5 and 6, the ambient room temperature was maintained constant throughout each run, and the calorimeter in equilibrium with the laboratory conditions. The slight discrepancy between the two runs in the steady-state temperature and heat-flow levels

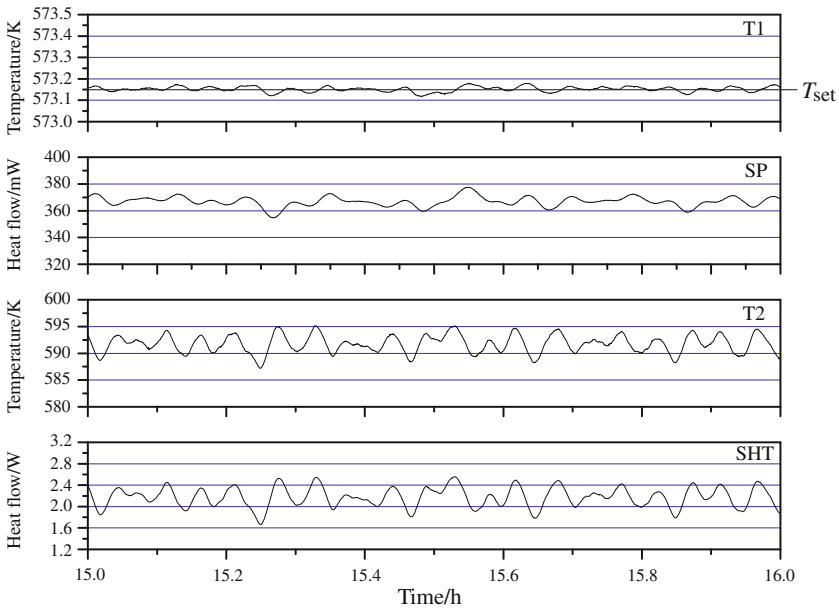

Fig. 5 System response during CTC-T1 control

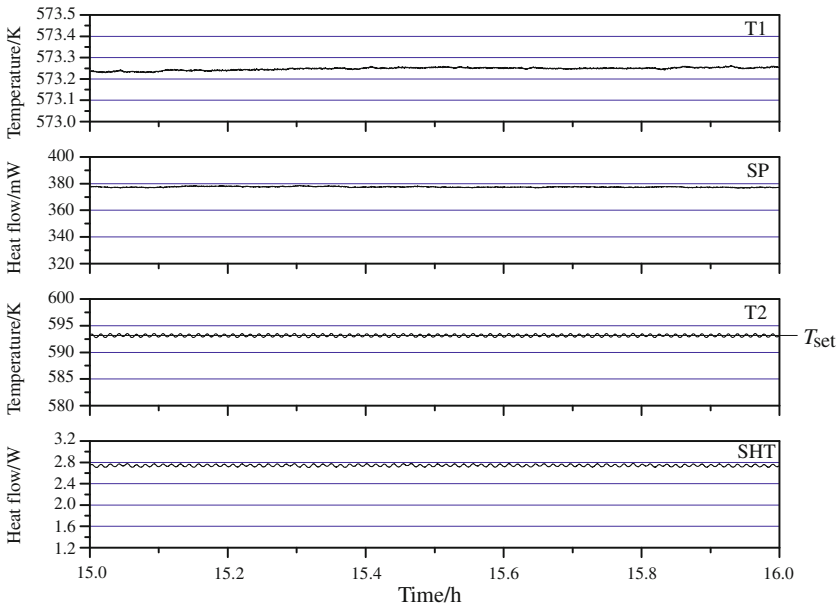

Fig. 6 System response during CTC-T2 control

indicates there is a small difference in room temperature during each run. Depending on the type of control used, as will be shown in a later section, achieving a steady condition in the temperature and stable heat flow readings may not be possible if the room temperature changes during a measurement.

System response to switchover between CTC-T2 and HFC-SHT schemes

The T1- and T2-temperature values, and SP- and SHT-heat-flow traces, are now depicted in Fig. 7 to compare the performance of the CTC-T2 control against the heat-flow-based control strategy that was reported in Vilchiz et al. [19]. The PID heat-flow control scheme (HFC-SHT), which was based on information collected by the SHT sensor, had the objective of regulating the heat flow, Q, supplied to the calorimeter core. Although its control loop is not shown here, the structure is identical to that of the CTC-T2 control scheme depicted in Fig. 3, the main difference being the information, Q instead of T, handled to/from the HFC-SHT controller.

In this run, CTC-T2 control was achieved and maintained over a 7 h period ($t \leq 7$ h), at the set-point $T_{set} = 593.15$ K, whereupon the control scheme was switched to HFC-SHT for $t > 7$ h, using a set-point value for the heat flow equal to the SHT sensor output of 2.75 W, which was the approximate steady-state value achieved by T2 during the $0 < t \leq 7$ h interval. For these conditions, the T1 value is equal to 573.25 K. The figure shows that after a brief transition period ($t < 15$ min) due to switch-over, thermal oscillations due to power cycling are resumed at very small amplitudes by either controller. Again, given the close proximity of the T2- and SHT-sensors to the electric heater, there will be little thermal lag and their response to the control actions, faster. Thermal averaging in the calorimeter core precludes the appearance of a transient in T1 during switch-over. In summary there is a general advantage of control via sensing close to the heater, whether by temperature measurement, or by heat-flow control sensing. It is to be noted that, after the transition period from the switch-over, there is an insignificant decline in the temperature readings for both T1 and T2, since the newly established set-point heat-flow value was slightly lower than the true steady-state value required to maintain T2 (under CTC-T2) at 593.15 K.

A direct comparison amongst the temperature- and heat-flow-based control schemes is shown in Fig. 8 for the two quantities of interest: the baseline signal SP, and the core temperature T1, during an 1-h period experiment. For clarity purposes, in both figures the signals obtained by CTC-T2 and HFC-SHT have been shifted vertically to start at the average value of the traces obtained by CTC-T1 control. It can be seen that although the heat-flow signals, as captured by the SP sensor, are maintained at averaged steady values by all the controllers, the CTC-T2 strategy provides a 20-fold reduction of peak-to-peak noise thermal cycling with respect to the 0.023 W p–p present with the control scheme based on information of the core temperature, and comparable to that of the heat-flow control. The oscillations present in CTC-T2 and HFC-SHT are due to the SSR actuator, whereas those of the CTC-T1 are mainly due to thermal lag since the sensor is farther from the heater. This behavior is reflected in the T1 signals, with the

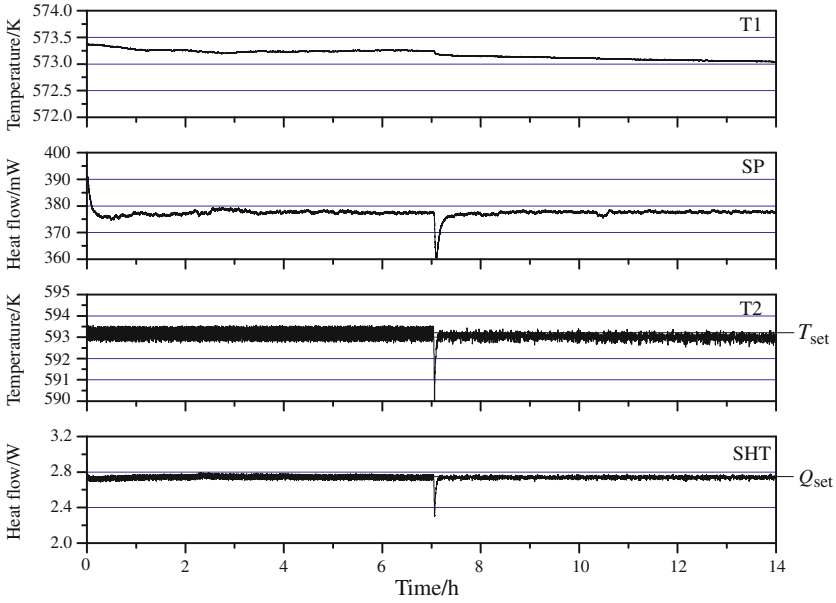

Fig. 7 Change in system response for a switchover from CTC-T2 for $t < 7$ h to HFC-SHT for $t \geq 7$ h

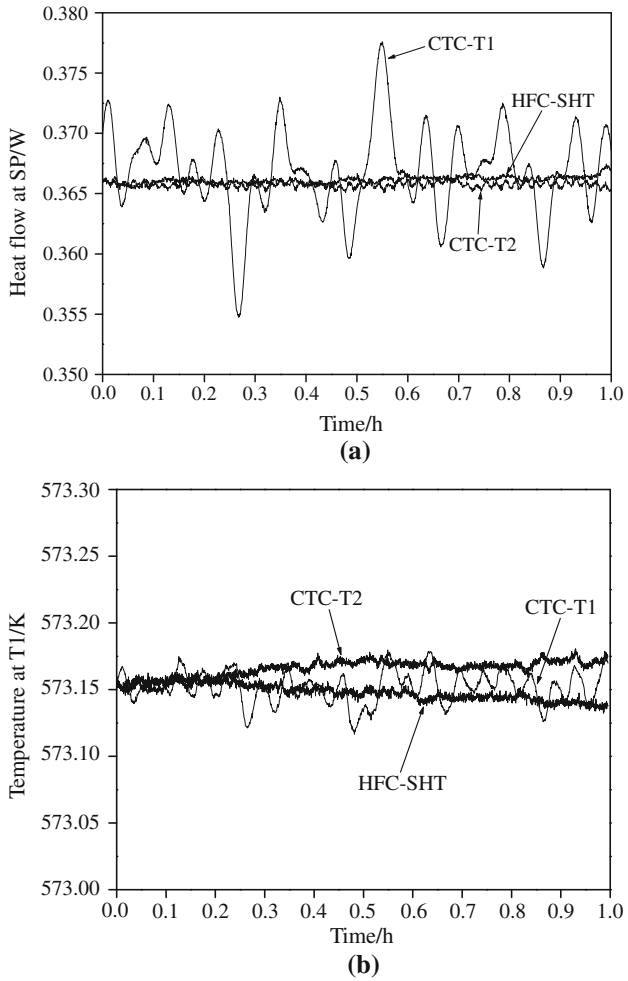

Fig. 8 Comparison of the short-term baseline stability provided by different control schemes. **a** Heat flow at SP location. **b** Core temperature at T1 location

main difference being that both temperature control strategies are more accurate than the HFC-SHT control in maintaining the core temperature at steady values.

System response to external variations during CTC-T2 control

Up to this point, it has been demonstrated that locating the control sensor closer to the actuator (heater) provides higher-quality information (reduced thermal lag), and hence a more precise control of the baseline stability. The reduction in the magnitude of the heater-induced oscillations are comparable to that of a previously reported heat-flow control strategy, and at least one order of magnitude better than that of the temperature control at the core (CTC-T1). We now test the robustness of the CTC-T2 temperature control strategy when external perturbations are present.

Figure 9 illustrates the dynamic response of the calorimeter to variations in the temperature external to the system when the CTC-T2 control strategy is applied. Shown are the signals corresponding to the controller output u_T (input voltage supplied by the actuator to the electric heater), the temperature values at locations T1 and T2, and the heat-flow signals captured by the SP- and SHT-sensors, all of which were collected during a time interval of 20 h. The test covers the period of inactivity in the lab, hence very subtle but important variations due to room air circulation and ambient temperature are evident. At the beginning of the experiment the lab street exit door was opened and left ajar for a period of 6 h, after which it was closed during an interval of 12 h, then re-opened for the remaining of the test. The temperature set-point at T2 was

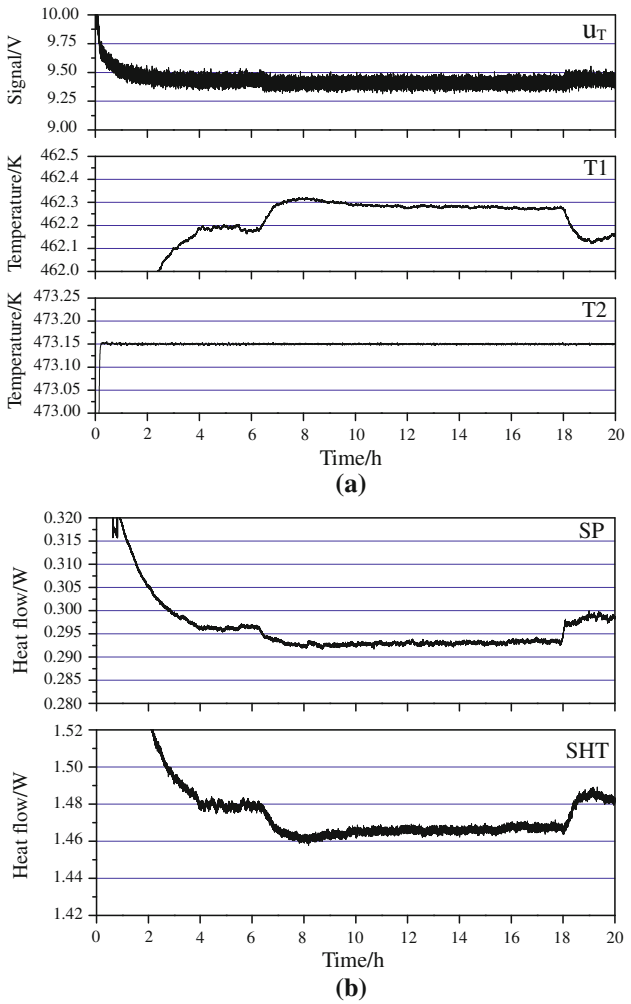

Fig. 9 System response to external variations in temperature under CTC-T2 control. **a** Time evolution of temperatures at T1 and T2, and controller output. **b** Time evolution of heat-flow traces as measured by SP and SHT sensors

fixed at 473.15 K. From the figure it can be seen that during the initial 2 h period, the actuator is adjusting power levels as the calorimeter approaches steady-state heat transfer with its surroundings, although it can be noticed that T2 achieves the set-point value within 10 min. Throughout the entire experiment the control actions are subtle, but evident in both the output signal voltage and T2 temperature traces, the latter being maintained at the set-point with peak-to-peak noise levels 0.01 K.

At the core, on the other hand, the corresponding T1 temperature stabilizes at 462.18 K after an initial transitory period of 4 h. When the door is closed, two hours later, the core temperature then increases to a maximum value of 462.33 K, after which the readings slowly decrease due to convective losses to the isolated room. Finally, a further drop in the temperature values to previous levels occurs again when the lab door is re-opened. The important observation here is that while the heater provides values of the heat input slightly adjusted to the closing/opening of the door, and T2 is being controlled within 0.005 K of its set-point value (c.f. Fig. 9), the core temperature T1 is changing with the external stimulus, the heat-flow signals at SP and SHT showing a mirror image of the T1 traces.

In fact, close inspection of the traces show that T1 and the sample-cup heat-flow (SP) respond simultaneously and ahead of SHT and the $u_T(t)$ controller output signals. The delay and slower response of SHT relative to SP (and to T1) is due to the fact that this sensor is embedded farther from the exterior walls of the calorimeter. The diminished but sustained heat flow levels of both SP and SHT, during the 12 h period that the lab door was closed, clearly illustrate that the controller has responded by slightly lowering the heater power to maintain the T2 setpoint level. The 0.1 K positive shift in the core temperature (T1) can be explained in terms of an increase in the total thermal resistance between the T1-location and the external environment (which includes the convective heat-transfer coefficient to the room), due to diminished air currents with the closed lab door. The higher air temperature then ensures a decrease of heat losses in calorimeter. Thus, in spite of maintaining the T2 level, T1 will increase in direct relation to the increased resistance of T1-to-exterior. It is obvious, therefore, that in the present configuration the temperature and heat flow levels cannot be controlled independently. As shown in Vilchiz et al. [19], the converse situation would apply if heat-flow control were used with the SHT sensor, and the sample-cup baseline heat-flow level would be held steady at the expense of temperature stability.

By looking at Figs. 4 and 9 it can be seen that the temperatures at T1 and T2 can be linked to the heat-flow values at SHT, Q_{SHT}, and hence to those at SP. A specific relationship between these is given as

$$Q_{\mathrm{SHT}} = \mathscr{K}(\mathrm{T2} - \mathrm{T1}), \tag{2}$$

where $\mathscr{K}$ is a calibration constant. This equation may be regarded as an approximation to the heat flow through SHT and associated temperatures at both ends of the sensor. After a calibration experiment, the core temperature can then be found from measurements of T2 and Q_{SHT}, as

$$\mathrm{T1^p} = \mathrm{T2} - \frac{Q_{\mathrm{SHT}}}{\mathscr{K}}, \tag{3}$$

where 'p' denotes the predicted value of T1.

An example of this fact is given in Fig. 10, which shows a comparison between the predicted and experimental values of the temperature at T1 for a step change in T2 from 373.15 to 533 K under CTC-T2 control. As observed from the figure, the difference between experiments and predictions is close to zero.

The aforementioned results indicate that it may be possible to build a control scheme that may satisfy simultaneously the

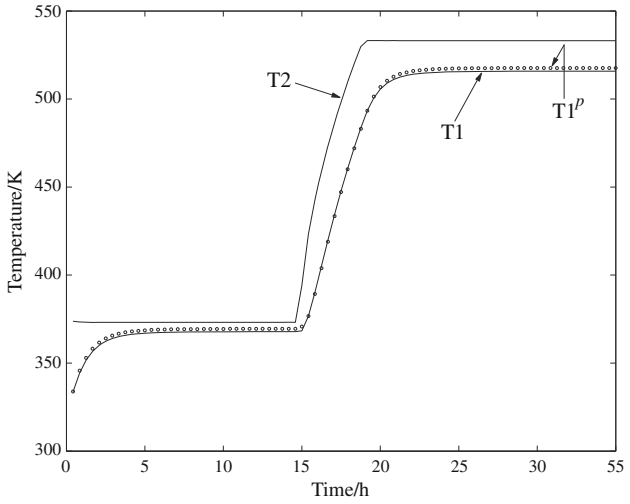

Fig. 10 Core temperature at T1. (−) Experiments; (○) Predictions from Eq. 3

two objectives of providing minimal heat-flow noise at the sample cup while maintaining an isothermal core by providing information about the temperature at T2 and the heat flow at SHT. Two multi-objective control strategies are currently under investigation.

Concluding remarks

Results from experimental tests have confirmed that sensor placement plays a fundamental role in the control of the calorimeter baseline stability and that it is better to place the sensing device closer to the heater than to the central core. Using information from a thermocouple located close to the actuator, the reduction in the magnitude of the heater-induced oscillations achieved by this control strategy is at least one order of magnitude better than that of the temperature control at the core, and comparable to the heat-flow control previously reported.

The general advantage of control via sensing close to the heater, whether by temperature measurement or by heat-flow control sensing, does not hold when external environmental disturbances to the calorimeter are present. When room air temperature and circulation currents change, the temperature and heat flow levels cannot be controlled independently with the control schemes presented here, and further investigation will focus on a multi-objective control strategy. A simultaneous sampling of both temperature and heat-flow values close to the electric heater may provide minimal thermal noise at the sample cup while maintaining an isothermal calorimeter core.

Acknowledgements Luis E. Vilchiz-Bravo was the recipient of a CONACyT Scholarship from Mexico for which we are grateful. This study has been partially supported by CONACyT 35106U and PROMEP/PTC-68 from Mexico, and by NSF IIP-0724505, IIP-0844891, and HRD-0932421 from the USA. The authors specially thank D. Loren and N. D. Green (I.T.I. company) for their assistance throughout this project.

References

1. Gravelle PC. Heat-flow microcalorimetry and its application to heterogeneous catalysis. Adv Catal. 1972;22:191–263.
2. Gravelle PC. Calorimetry in adsorption and heterogeneous catalysis studies. Catal Rev Sci Eng. 1977;16(1):37–110.
3. Handy BE, Sharma SB, Spiewak BE, Dumesic JA. A Tian-Calvet heat-flux microcalorimeter for measurement of differential heats of adsorption. Meas Sci Technol. 1993;4:1350–56.
4. Hansen LD. Calorimetric measurement of the kinetics of slow reactions. Ind Eng Chem Res. 2000;39:3541–49.
5. Cardona-Martinez N, Dumesic JA. Applications of adsorption microcalorimetry to the study of heterogeneous catalysis. Adv Catal. 1992;38:149–244.
6. Auroux A. Microcalorimetry methods to study the acidity and reactivity of zeolites, pillared clays and mesoporous material. Topic Catal. 2002;19:205–13.
7. Hart MP, Brown DR. Surface acidities and catalytic activities of acid-activated clays. J Mol Catal A: Chem. 2004;212:315–21.
8. Ostrovskii VE. Review of the heats of chemisorption of gases at metals in the context of the problem of 'Heterogeneous' vs. 'Homogeneous' catalytic surfaces. J Therm Anal Calorim. 2009;95:609–22.
9. Dragoi B, Rakic V, Dumitriu E, Auroux A. Adsorption of organic pollutants over microporous solids investigated by microcalorimetry techniques. J Therm Anal Calorim. 2010;99:733–40.
10. Parrillo DJ, Gorte RJ. Design parameters for the construction and operation of heat-flow calorimeters. Thermochim Acta. 1998;312:125–32.
11. Hansen LD, Eatough DJ. Comparison of the detection limits of microcalorimeters. Thermochim Acta. 1983;70:257–68.
12. Garcia-Cuello V, Moreno-Pirajan JC, Giraldo-Gutierrez L, Sapag K, Zgrablich G. Variation of the noise levels in the baseline of an adsorption microcalorimeter. J Therm Anal Calorim. 2009;97:705–9.
13. Inaba H, Takahashi S, Mima T, Naito K. A high temperature Tian-Calvet type calorimeter and an analysis of the baseline fluctuation. J Chem Thermodyn. 1984;16:573–82.
14. Ostrovskii VE. Molar heats of chemisorption of gases at metals: review of experimental results and technical problems. Thermochim Acta. 2009;489:5–21.
15. Vilchiz LE, Pacheco-Vega A, Handy BE. Heat-flow patterns in Tian-Calvet microcalorimeters: conductive, convective, and radiative transport in gas dosing experiments. Thermochim Acta. 2005;439:110–8.
16. Garcia-Cuello V, Moreno-Pirajan JC, Giraldo-Gutierrez L, Sapag K, Zgrablich G. Design, calibration, and testing of a new Tian-Calvet heat-flow microcalorimeter for measurement of differential heats of adsorption. Instrum Sci Technol. 2008;36:455–75.
17. Hemmerich JL, Serio L, Milverton P. High-resolution tritium calorimetry based on inertial temperature control. Rev Sci Instrum. 1994;65:1616–20.
18. Velazquez-Campoy A, Lopez-Mayorga O, Cabrerizo-Vilchez MA. Development of an isothermal titration microcalorimetric system with digital control and dynamic power Peltier compensation. I. Description and basic performance. Rev Sci Instrum. 2000;71:1824–31.
19. Vilchiz-Bravo LE, Pacheco-Vega A, Handy BE. Heat-flow and temperature control in Tian-Calvet microcalorimeters: toward

higher detection limits. Meas Sci Technol. 2010. doi: 10.1088/0957-0233/21/11/115103.
20. Vilchiz-Bravo LE. Heat transfer numerical simulations and control strategies to improve thermal sensitivity in Tian-Calvet calorimeters (in Spanish). PhD Thesis, Universidad Autónoma de San Luis Potosí, México. 2007.
21. Pacheco-Vega A, Ruiz-Mercado C, Peters K, Vilchiz-Bravo L. On-line fuzzy-logic-based temperature control of a concentric-tube heat exchanger facility. Heat Transf Eng. 2009;30:1208–15.
22. Díaz G, Sen M, Yang KT, McClain RL. Dynamic prediction and control of heat exchangers using artificial neural networks. Int J Heat Mass Transf. 2001;44:1671–79.
23. Kubrusly CS, Malebranche H. Sensors and controllers location in distributed systems—a survey. Automatica. 1985;21:117–28.
24. Tarabanis KA, Allen PK, Tsai RY. A survey of sensor planning in computer vision. IEEE Trans Robotics Autom. 1995;11:86–104.
25. Uciński D. Optimal sensor location for parameter estimation of distributed processes. Int J Control. 2000;73:1235–48.
26. Abidi B, Aragam N, Yao Y, Abidi M. Survey and analysis of multimodal sensor planning and integration for wide area surveillance. ACM Comput Surv. 2008;41:1–36.
27. Arbel A. Controllability measures and actuator placement in oscillatory systems. Int J Control. 1981;33:565–74.
28. Ning HH. Optimal number and placements of piezoelectric patch actuators in structural active vibration control. Eng Comput. 2004;21:651–665.
29. Franco W, Sen M, Yang KT. Optimization of control hardware placement in a thermal-hydraulic network. HVAC R Res. 2008;14:73–84.
30. Worden K, Burrows AP. Optimal sensor placement for fault detection. Eng Struct. 2001;23:885–901.
31. Meo M, Zumpano G. On the optimal sensor placement techniques for a bridge structure. Eng Struct. 2005;27:1488–97.
32. Yao Y, Chen CH, Abidi B, Page D, Koschan A, Abidi M. Can you see me now? Sensor positioning for automated and persistent surveillance. IEEE Trans Sys Man Cyber-B. 2010;40:101–15.
33. Reda S, Cochran RJ, Nowroz AN. Improved thermal tracking for processors using hard and soft sensor allocation techniques. IEEE Trans Comput. 2011;60:841–51.